Engineering Structures 151 (2017) 472–487

Contents lists available at ScienceDirect

Engineering Structures

journal homepage: www.elsevier.com/locate/engstruct

Stress-strain model for confined concrete with corroded transverse reinforcement

Ngoc Son Vu [a], Bo Yu [b], Bing Li [c,*]

[a] Department of Structural Mechanics, National University of Civil Engineering, Viet Nam
[b] Key Laboratory of Disaster Prevention and Structural Safety of China Ministry of Education, Guangxi Key Laboratory of Disaster Prevention and Engineering Safety, School of Civil Engineering and Architecture, Guangxi University, 530004, China
[c] School of Civil and Environmental Engineering, Nanyang Technological University, 639798, Singapore

ARTICLE INFO

Article history:
Received 21 March 2017
Revised 8 August 2017
Accepted 20 August 2017

Keywords:
Corroded confined concrete
Corroded transverse reinforcement
Corrosion level
Stress-strain relation

ABSTRACT

This paper presents an experimental study on the stress-strain relation of confined concrete that considers the corrosion effects of transverse reinforcement. The main variables are the corrosion level of transverse reinforcement, cross sectional shape of confined concrete, as well as arrangement and configuration of confining transverse reinforcing bars. The test results revealed that four key parameters of the complete stress-strain relation are significantly affected due to the corrosion of transverse reinforcement, including the maximum concrete strength and corresponding axial concrete strain, maximum concrete strain at the fracture of the first hoops, and descending branch of the stress-strain curve after exceeding the maximum strength. Based on the test data and regression analysis, the empirical equations to estimate these key parameters are proposed, and a complete stress-strain model for confined concrete with corroded transverse reinforcement is developed. The proposed model showed good correlation with the test data of both circular and square specimens with various corrosion levels and subjected to compression axial loading.

1. Introduction

Corrosion of steel reinforcement has been found to be one of the most significant causes of deteriorations for reinforced concrete (RC) structures subjected to various corrosive environmental actions. The corrosion products expand the volume of corroded steel reinforcement that develops the tensile stresses at the interfacial regions between reinforcement and concrete, causing the cover concrete of these RC structures to crack and spall off [1]. Additionally, the deterioration of strength and ductility of reinforcement due to corrosion also results in the significant reduction of the confinement effectiveness for confined concrete and buckling resistance of longitudinal reinforcement. As a result, the durability and safety performance of RC structures will be adversely affected especially important since these structures usually exist in the severely corrosive environments and earthquake prone regions [2,3].

Past earthquakes have proved that inadequate confinement of core concrete results in brittle characteristics under severe earthquake which should be avoided in design. The amount and arrangement of confining transverse reinforcement play a significant role in enhancing the performance of RC structures, especially in their inelastic ranges. During the service life of RC structures, their strength and ductility often deteriorate due to reinforcement corrosion, hence these deteriorations should be accurately predicted and taken into account from the outset of the design process, even more so for structures built in corrosive environments and subjected to seismic loading. In literature, the behavior of reinforced concrete beams with corroded reinforcement has been well investigated, particularly their flexural and shear strength deteriorations due to corrosion of reinforcement [4–7]. In addition, there are also several experimental studies about the effects of corrosion on the performance of RC columns subjected to seismic loading. Particularly, studies conducted by Meda et al. [8], Yang et al. [9], and Goksu and Ilki [10] were devoted to investigate the effects of corrosion on the seismic behavior of RC columns which failed in flexural manners while the other studies carried out by Bousias et al. [11], Li et al. [12], and Meda et al. [13] have focused on the effectiveness of strengthening methods on corroded RC columns subjected to cyclic loading. It is also clearly recognized that the stress-strain relations of reinforcement and confined concrete material are important input parameters to predict the performance of RC members, particularly their flexural and shear

* Corresponding author.
E-mail address: CBLI@ntu.edu.sg (B. Li).

http://dx.doi.org/10.1016/j.engstruct.2017.08.049
0141-0296/

Nomenclature

D_0	original diameter of reinforcement
$D_{\min}$	minimum residual diameter of corroded reinforcement
D_{re}	average residual diameter of corroded reinforcement
E_c	elasticity modulus of concrete
E_{sec}	secant modulus of confined concrete at maximum stress
E_{stress}	normalized corroded concrete stress error
f_c	longitudinal concrete stress
f'_c	compressive strength of standard concrete cylinder specimens
f'_{cc}	compressive strength of corroded confined concrete
$f'^{\exp}_{cc}$	measured compressive strength of corroded confined concrete
f'^{pro}_{cc}	calculated compressive strength of corroded confined concrete using Eq. (15)
f'_{co}	compressive strength of unconfined concrete
f'_l	effective lateral confining stress
f_y	yield strength of longitudinal reinforcement
f_{yh}	yield strength of transverse reinforcement
f^c_{yh}	yield strength of corroded transverse reinforcement
F_{mea}	measured corroded concrete stress
F_{cal}	calculated corroded concrete stress
k_e	confinement effectiveness coefficient
l_i	length of the crack i
L	clear height of column
p_0	perimeter of specimen cross section
X_{corr}	corrosion level in terms of mass loss
$X^{(1)}_{corr}$	corrosion level in terms of average residual cross sectional area
$X^{(2)}_{corr}$	corrosion level in terms of minimum residual cross sectional area
w_{cri}	width of crack i
W_{cr}	total crack width of the specimen
W_0	original weight of reinforcement before corrosion
W_1	residual weight of reinforcement after corrosion
α	stress correction coefficient
α_s	yield strength reduction factor for corroded transverse reinforcement
β	strain correction coefficient
β_s	ultimate strain reduction factor for corroded transverse reinforcement
ε_c	longitudinal concrete strain
ε_{cc}	corroded concrete strain at maximum concrete stress
$\varepsilon^{\exp}_{cc}$	measured corroded concrete strain at maximum concrete stress
ε^{pro}_{cc}	calculated corroded concrete strain at maximum concrete stress using Eq. (16)
ε_{cu}	ultimate strain of corroded confined concrete
$\varepsilon^{\exp}_{cu}$	measured ultimate strain of corroded confined concrete
ε^{pro}_{cu}	calculated ultimate strain of corroded confined concrete using Eq. (17)
ε_{sm}	steel strain at maximum tensile stress of transverse reinforcement
ε^c_{sm}	steel strain at maximum tensile stress of corroded transverse reinforcement
ρ_s	volumetric ratio of transverse reinforcement of uncorroded confined concrete
ρ_{sc}	volumetric ratio of transverse reinforcement of corroded confined concrete

behavior. While the stress-strain relations for corroded reinforcement have been well studied in literature [14–20], to the authors' knowledge, so far there is no analytical stress-strain model for confined concrete with corroded transverse reinforcement. In this study, the stress-strain relation of confined concrete with various corrosion levels of transverse reinforcement has been experimentally investigated. Meanwhile, the influences of corrosion level of transverse reinforcement on the characteristic parameters of the stress-strain relation are investigated. Finally, an analytical stress-strain model for confined concrete with corroded transverse reinforcement is proposed based on the experimental data by incorporating the corrosion effects into the model for uncorroded confined concrete suggested by Mander et al. [21].

2. Experimental program

2.1. Test specimens

This experimental study included 36 reinforced concrete columns with 600 mm in height which were either 200 mm square or 200 mm diameter circular sections, with cover concrete thickness of 10 mm. Fig. 1 shows the arrangements of longitudinal reinforcing bars, transverse hoops, square helices, and spiral reinforcement of the specimens. As indicated, the test specimens were divided into three series: Series A (AS, AM, AL), Series B (BS, BM, BL), and Series C (CS, CM, CL) that represent different cross sectional shapes, various arrangements of longitudinal and transverse reinforcing bars. Following which the specimens in each series were corroded with different corrosion levels by controlling the accelerated corrosion time and the applied current intensity. The reinforcement details of the square and circular test specimens are summarized in Table 1.

In order to make sure that test specimens fail in the middle regions, the spacing of transverse reinforcement was decreased to 25 mm within the regions of 100 mm from both ends of the specimens to provide more confinement effect in these regions. To prevent the spalling of cover concrete at both ends of the specimens because of the stress concentration and corrosion attacks, the external confinement using the steel frames was also installed in two end regions of the specimens, as demonstrated in Figs. 1 and 3.

2.2. Material properties

The target concrete strength of 30 MPa for test specimens was supplied by a local ready-mix plant and casted in five batches. Three 150 × 300 mm cylinder specimens and an unconfined concrete specimen were made for each batch. The unconfined concrete specimens have the same dimension as the other specimens, however, without transverse reinforcement, that is 600 mm in height and either 200 mm square or 200 mm circular sections, which were tested to estimate the maximum strength and the corresponding axial strain for unconfined concrete. The average compressive strengths of the cylinders at testing days, above 28 days, for the five batches of specimens were 30.5, 29.3, 25.9, 25.3, and 31.9 MPa while the corresponding strengths of the unconfined concrete specimens were 25.4, 24.9, 21.7, 18.0, and 24.4 MPa, respectively. The axial concrete strain of unconfined concrete at maximum stress for each batch of specimens was also recorded, as indicated in Table 1. As a result of the size effect and less effective consolidation, the maximum strength of unconfined concrete

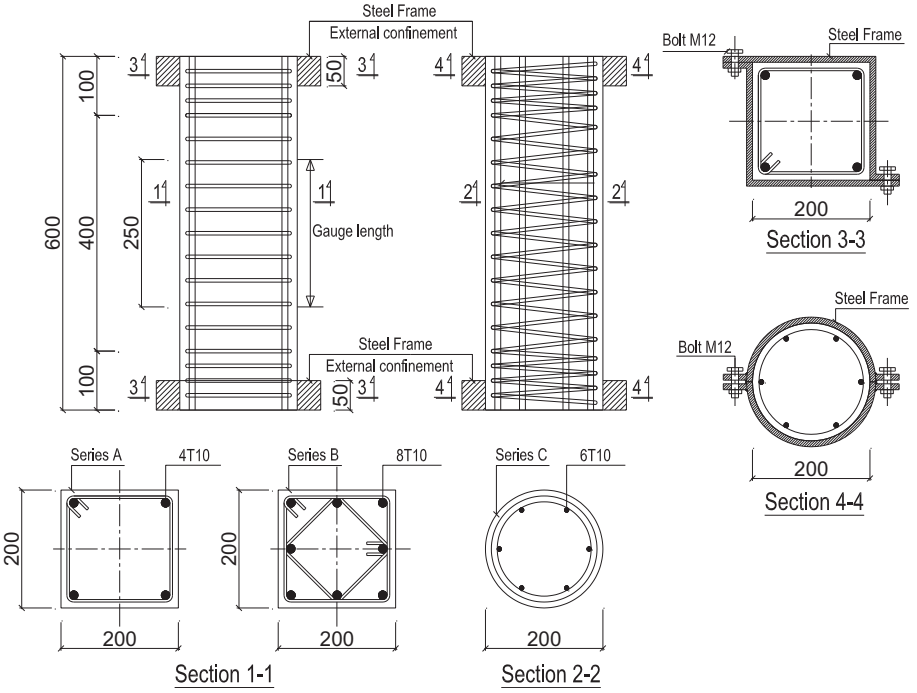

Fig. 1. Details of test specimens (note: all dimensions are in mm).

Table 1
Specimen properties and corrosion measurement.

Unit	Plain concrete data			Longitudinal reinforcement			Transverse reinforcement				Corrosion level			Total crack width (mm)
	f'_c (MPa)	f'_{co} (MPa)	ε_{co}	No. (bars)	Dia. (mm)	f_y (MPa)	Dia. (mm)	Spa. (mm)	f_{yh} (MPa)	ρ_s (%)	X_{corr} (%)	$X^{(1)}_{corr}$ (%)	$X^{(2)}_{corr}$ (%)	
AL0	30.5	25.4	0.0016	4	10	568	6	65	360	0.97	0.0	0.0	0.0	0.00
AL1	30.5	25.4	0.0016	4	10	568	6	65	360	0.97	4.9	10.8	23.8	0.00
AL2	30.5	25.4	0.0016	4	10	568	6	65	360	0.97	9.8	18.9	36.9	0.12
AL3	30.5	25.4	0.0016	4	10	568	6	65	360	0.97	17.5	30.7	53.7	0.48
AM0	30.5	25.4	0.0016	4	10	568	6	40	360	1.57	0.0	0.0	0.0	0.00
AM1	30.5	25.4	0.0016	4	10	568	6	40	360	1.57	7.3	6.7	18.9	0.00
AM2	30.5	25.4	0.0016	4	10	568	6	40	360	1.57	12.5	17.4	36.6	0.21
AM3	30.5	25.4	0.0016	4	10	568	6	40	360	1.57	21.6	41.1	73.6	0.71
AS0	29.3	24.9	0.0015	4	10	568	6	25	360	2.51	0.0	0.0	0.0	0.00
AS1	29.3	24.9	0.0015	4	10	568	6	25	360	2.51	9.5	13.8	41.6	0.13
AS2	29.3	24.9	0.0015	4	10	568	6	25	360	2.51	16.7	14.3	53.3	0.44
AS3	29.3	24.9	0.0015	4	10	568	6	25	360	2.51	25.0	26.6	76.8	1.10
BL0	29.3	24.9	0.0015	8	10	568	6	65	360	1.65	0.0	0.0	0.0	0.00
BL1	29.3	24.9	0.0015	8	10	568	6	65	360	1.65	7.7	10.7	35.0	0.00
BL2	29.3	24.9	0.0015	8	10	568	6	65	360	1.65	10.3	18.1	59.9	0.15
BL3	29.3	24.9	0.0015	8	10	568	6	65	360	1.65	12.3	19.4	58.8	0.41
BM0	25.9	21.7	0.0014	8	10	568	6	40	360	2.68	0.0	0.0	0.0	0.00
BM1	25.9	21.7	0.0014	8	10	568	6	40	360	2.68	5.6	5.9	17.6	0.00
BM2	25.9	21.7	0.0014	8	10	568	6	40	360	2.68	10.0	17.3	48.7	0.29
BM3	25.9	21.7	0.0014	8	10	568	6	40	360	2.68	13.4	30.4	50.5	0.27
BS0	25.9	21.7	0.0014	8	10	568	6	25	360	4.29	0.0	0.0	0.0	0.00
BS1	25.9	21.7	0.0014	8	10	568	6	25	360	4.29	14.9	26.3	56.5	0.35
BS2	25.9	21.7	0.0014	8	10	568	6	25	360	4.29	20.8	28.3	59.2	0.66
BS3	25.9	21.7	0.0014	8	10	568	6	25	360	4.29	25.0	34.6	79.1	0.90
CL0	25.3	18.0	0.0016	8	10	568	6	55	360	1.14	0.0	0.0	0.0	0.00
CL1	25.3	18.0	0.0016	8	10	568	6	55	360	1.14	16.8	15.1	31.8	0.45
CL2	25.3	18.0	0.0016	8	10	568	6	55	360	1.14	21.8	26.2	47.4	0.72
CL3	25.3	18.0	0.0016	8	10	568	6	55	360	1.14	31.5	40.6	85.4	1.25
CM0	31.9	24.4	0.0017	8	10	568	6	40	360	1.57	0.0	0.0	0.0	0.00
CM1	31.9	24.4	0.0017	8	10	568	6	40	360	1.57	7.6	5.7	24.3	0.00
CM2	31.9	24.4	0.0017	8	10	568	6	40	360	1.57	22.8	40.0	70.5	1.00
CM3	31.9	24.4	0.0017	8	10	568	6	40	360	1.57	32.9	44.5	89.1	1.50
CS0	31.9	24.4	0.0017	8	10	568	6	25	360	2.51	0.0	0.0	0.0	0.00
CS1	31.9	24.4	0.0017	8	10	568	6	25	360	2.51	9.3	8.3	28.0	0.20
CS2	31.9	24.4	0.0017	8	10	568	6	25	360	2.51	10.0	11.2	36.0	0.35
CS3	31.9	24.4	0.0017	8	10	568	6	25	360	2.51	13.6	19.0	47.3	0.60

was less than the expected 85% the strength of standard cylinder specimen. It is noted that to improve the electrical conductivity of concrete in the accelerated corrosion scheme, 5% sodium chloride (NaCl) by weight of cement was added into the concrete mixing ingredients. The experimental stress-strain relations of the original reinforcing bars are indicated in Fig. 2 and their mechanical properties are presented in Table 2.

2.3. Instrumentation

A 5000 kN capacity hydraulic testing machine was utilized to provide the concentric axial load using displacement control with the loading rate of 0.5 mm/min. A preload of 50 kN was applied to the specimens and the readings from the linear variable displacement transducers (LVDTs) and strain gauges were checked to ensure the specimens deform uniformly. Two different methods of recording axial deformations were used during testing of the specimens in this experimental program [22]. The first method was to measure the overall axial deformation of the specimen between the platen and the crosshead, that is, the gauge length is total height of the specimen, 600 mm, using the reading results of the hydraulic machine. The measured results of the first method will be used if localized failure does not happen at the central part of the specimen. The second method used two pairs of 25 mm LVDTs mounted on the opposite sides of the square specimens while three LVDTs were used for circular specimens, which were mounted on a pairs of aluminum hoops embedded in the mid-height of the specimens. The distance between two aluminum hoops is 250 mm. It was observed that the failure regions of all test specimens were at the central part of the specimen within the gauge length of 250 mm as predicted. Fig. 3 shows the typical test set-up of the square and circular specimens. The axial deformation of the specimens was then derived from the average readings of the LVDTs. A pair of concrete strain gauges was also attached on the surface of the specimens to measure the axial concrete strain in the elastic range of concrete. The experimental results revealed that the readings of the concrete strain gauges exactly coincided with the readings of the LVDTs in the elastic range of the specimens. In this study, it is also noted that there are no strain gauges installed on the reinforcing bars as they will be damaged by the accelerated corrosion process.

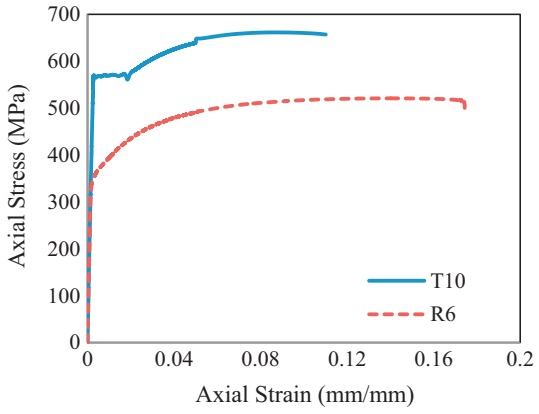

Fig. 2. Typical stress-strain curves of reinforcement.

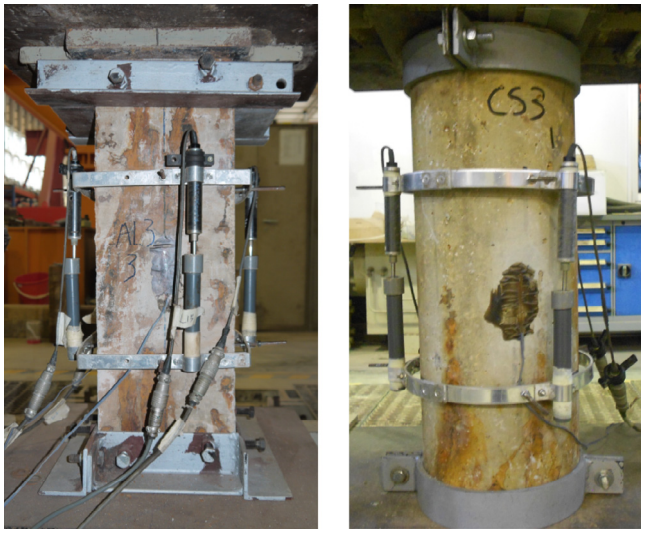

Fig. 3. Typical test set-up of square and circular specimens in 5000 kN capacity hydraulic universal testing machine.

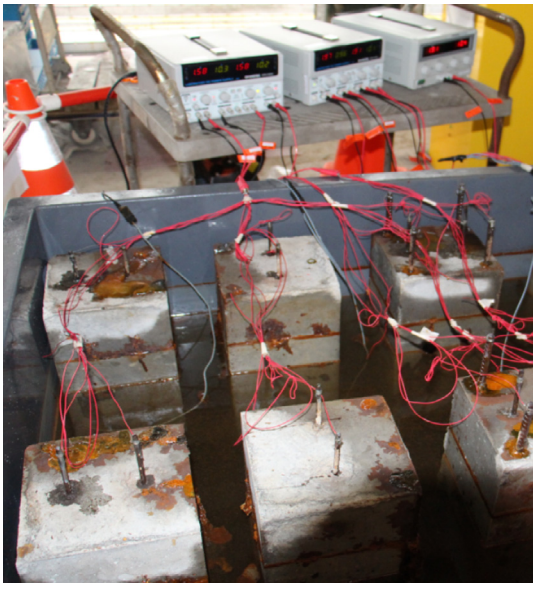

Fig. 4. Accelerated corrosion scheme.

2.4. Accelerated corrosion scheme

The electro-chemical method was adopted to accelerate corrosion process in reinforced concrete specimens, due to the fact that the natural corrosion process usually takes several years or decades. Transverse reinforcing bars were corroded using an electro-chemical method and a constant current density of approximately

Table 2
Properties of reinforcement.

Steel type	Nominal diameter (mm)	Yield strength (MPa)	Ultimate strength (MPa)	Modulus of elasticity (GPa)
R6	6	360.0	525.4	210
T10	10	568.3	654.5	210

0.5 mA/cm^2 was applied to the transverse reinforcing bars by connecting to the anodes of the DC power supplies while their cathodes were connected to the copper plates. To simulate the corrosive environments, the specimens were immersed in the water tank with a 5% sodium chloride (NaCl) solution, as shown in Fig. 4. The longitudinal reinforcing bars were not corroded in this study and isolated from the transverse reinforcement by using the electrical tapes. In theory, the corrosion level of reinforcement in terms of mass loss can be estimated by using the Faraday's law and governed by the accelerated corrosion time. However, many researchers pointed out that the Faraday's law overestimates the corrosion level of reinforcement and this finding is also confirmed in this experimental program. Therefore, in this study, the corrosion level was estimated based on the measured data of experiment as presented in the following section.

2.5. Corrosion level assessment

It is well known that the corrosion degree of reinforcement can be evaluated in terms of either mass loss or residual cross-sectional area. In this study, three evaluation methods of corrosion degree of reinforcement based on experimental measurement are proposed, including corrosion levels in terms of mass loss X_{corr}, average residual cross sectional area $X^{(1)}_{corr}$, and minimum residual cross sectional area, or pitting corrosion $X^{(2)}_{corr}$, defined as follows:

$$X_{corr} = \frac{W_0 - W_1}{W_0} \tag{1}$$

$$X^{(1)}_{corr} = \frac{D_0^2 - D_{re}^2}{D_0^2} \tag{2}$$

$$X^{(2)}_{corr} = \frac{D_0^2 - D_{\min}^2}{D_0^2} \tag{3}$$

where W_0 and D_0 are the original weight and diameter of reinforcement before corrosion; W_1, D_{re}, and $D_{\min}$ are the residual weight, average residual diameter, and minimum residual diameter of reinforcement after corrosion, respectively. The measurement procedure follows ASTM G1-03 [23] particularly after testing, all the reinforcing bars were taken out of the test specimens and then were cleaned by the steel brushes. After that, they were immersed in 10% hydrochloric acid (HCl) for 20 min to remove all the rust, as demonstrated in Fig. 5. Finally, all the reinforcing bars were measured to estimate their weight loss and residual diameters. It should be noted that all transverse reinforcing bars were weighed before doing formwork and concrete casting to estimate the original weight of all transverse reinforcing bars. In order to measure the average and minimum residual diameters (or pitting corrosion) along the length of the transverse reinforcing bars, the transverse reinforcement was equally divided into eight regions, four regions at the corners, and the other four regions at the middle of steel reinforcement, then the average and minimum residual diameters of each transverse reinforcement were recorded. The digital vernier caliper was used to measure the minimum residual diameters of the corroded reinforcement. Firstly, eight regions of each transverse reinforcing bar were measured to obtain their minimum residual diameters. After that, the minimum residual diameter of each transverse reinforcing bar is obtained by taking the minimum value among these obtained values of eight regions. The same measurement procedure was repeated for all transverse reinforcing bars. Finally, the minimum residual diameter of transverse reinforcement of the specimen is achieved by taking the average value of minimum residual diameters of all transverse reinforcing bars. The measured corrosion levels of transverse reinforcement of test specimens are tabulated in Table 1. In this experimental program, there is relatively high correlation between corrosion level in terms of minimum residual cross sectional area and corrosion level in terms of mass loss of corroded specimens, as indicated in Fig. 6. In addition, the correlative relationship between corrosion level in terms of average residual cross sectional loss and average corrosion level in terms of mass loss of corroded specimens is also demonstrated in Fig. 7. Although the test results show that the cross-sectional loss varies along the length of the transverse reinforcement, the measured mass loss and residual cross sectional area for different corroded transverse reinforcing bars are relatively comparable. It is due to the fact that all the transverse reinforcing bars were applied and remained the same constant current density of 0.5 mA/cm^2 during the accelerated corrosion process. Hence in this study, for convenience and simplification in calculation, the corrosion level in terms of mass loss is adopted to describe the corrosion degree of transverse reinforcement as well as develop the stress-strain model for confined concrete with corroded transverse reinforcement.

2.6. Corrosion cracks

After the accelerated corrosion, the corroded specimens subjected to low corrosion level, less than 10% in terms of mass loss, did not show any visible cracks. On the other hand, the cracks induced by corrosion were obvious for the specimens subjected to high corrosion level which primarily appeared and developed vertically along the direction of longitudinal reinforcement. Fig. 8

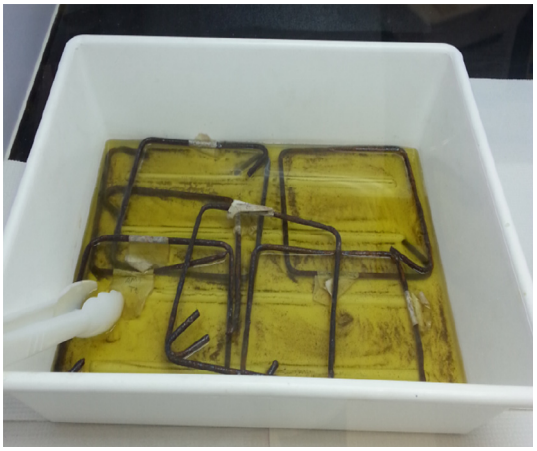

Fig. 5. Process of removing the rust from corroded reinforcement.

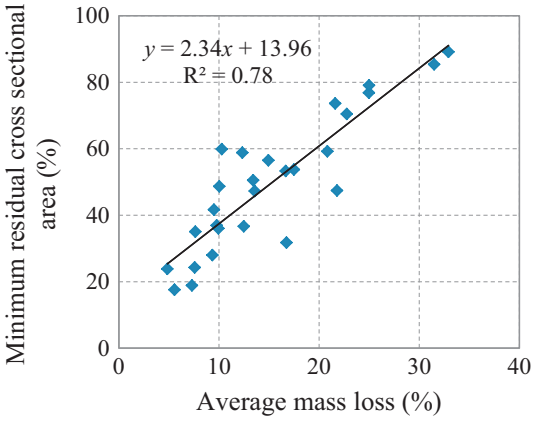

Fig. 6. Relationship between corrosion levels in terms of average mass loss and minimum residual cross sectional area of corroded specimens.

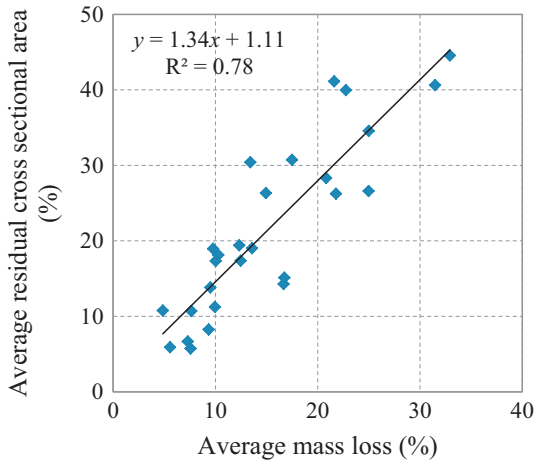

Fig. 7. Relationship between corrosion levels in terms of mass loss and average residual cross sectional area of corroded specimens.

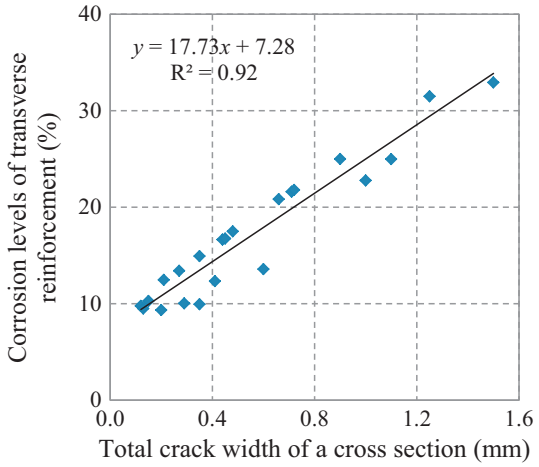

Fig. 9. Relationship between total crack width of a cross section and corrosion levels of transverse reinforcement of corroded specimens.

demonstrates some corroded specimens after accelerating corrosion process and cleaning all the rust on their surfaces.

Their width and length were traced and measured at all sides of the specimens using the crack width gauges. In order to consider the effect of cover concrete cracks to the stress-strain relations of corroded confined concrete, the total crack width of the specimen W_{cr} which is defined as the average value of crack width determined for the four sides of the test specimen as follows:

$$W_{cr} = \frac{\sum w_{cri} l_i}{L} \tag{4}$$

where w_{cri} is the width of crack i; l_i is the length of the crack i; L is the clear height of test specimens (L = 600 mm). The total crack width of the specimen of corroded specimens is indicated in Table 1. As observed, the total crack width increases with the increase of corrosion level. A good correlation between the total crack width of the specimen and the corrosion level of transverse reinforcement in terms of mass loss is shown in Fig. 9. It is noted that the total crack width W_{cr} of the specimen which is defined as Eq. (4) can be easily measured in the experiment and real engineering using the crack width gauges.

2.7. Measured stress-strain curves for confined concrete

In this study, it is noted that the test result from the hydraulic testing machine was the total load carried by the confined concrete with transverse reinforcement, unconfined cover concrete, and longitudinal reinforcing bars. Therefore, the longitudinal steel force and the cover concrete force contributions were subtracted to give the total load carried by the confined concrete which was divided by the core area to obtain the confined concrete stress [24,25]. The longitudinal steel force was calculated based on the tensile test results. In order to convert the measured stress-strain relations of reinforcement in tension into the stress-strain relations in compression, the steel model proposed by Dodd and Cooke [26] was adopted. For un-corroded specimens, the force contribution of the unconfined cover concrete was calculated by multiplying the concrete stress obtained from the unconfined concrete specimens f'_{co} (of the same size as the reinforced specimens) by the cover area of the reinforced concrete specimen. For the corroded specimens, the compressive concrete strength of cover concrete was reduced to $\zeta f'_{co}$ due to the cracks of cover concrete induced by corrosion and the softening coefficient ζ can be estimated as follows [27]:

$$\zeta = \frac{0.9}{\sqrt{1 + 600\varepsilon_r}} \tag{5}$$

$$\varepsilon_r = \frac{W_{cr}}{p_0} \tag{6}$$

where ε_r is the tensile strain induced by the cracks of cover concrete; W_{cr} is the total crack width of the specimen, as indicated in

Fig. 8. Appearance of corroded specimens after accelerated corrosion scheme.

Table 1 or predicted as Eq. (5) based on corrosion level in terms of mass loss of transverse reinforcement; p_0 is the perimeter of the column section. Fig. 10 demonstrates the experimental results of stress-strain curves for confined concrete of test specimens subjected to various corrosion levels.

3. General description of test behavior

The failure mode of test specimens are characterized sequentially by the appearance and propagation of vertical cracks along the longitudinal reinforcing bars, the cover concrete spalling after the specimens exceeded the peak stress, either the fracture of transverse reinforcement or the bucking of longitudinal reinforcing bars occurs first, depending on the spacing and corrosion levels of transverse reinforcement, and finally the crushing of core concrete. As observed in Fig. 10, the volumetric ratio of transverse reinforcement and the corrosion level are the most important parameters that significantly affect the stress-strain relations of corroded specimens for all cross sectional shapes, including maximum concrete strength and the corresponding axial strain, ultimate concrete strain, and the stress-strain curves after exceeding the maximum strength.

The experimental observation also revealed that the pitting corrosion becomes more significant with the increase of corrosion level. Particularly, for the corroded specimens with the corrosion level approximately less than 10%, it is observed that the diameter of transverse reinforcing bars of these specimens reduced relatively uniformly, generally defined as uniform corrosion. Fig. 11 demonstrates an example of some typical corroded transverse reinforcing bars of corroded Specimen AS1 with the corrosion level of 9.5% after testing and cleaning all the rust. In addition, the accelerated corrosion process of transverse reinforcement did not cause any visible cracks on the surface of these specimens. As a result of uniform corrosion and low corrosion level of transverse reinforcement, the overall stress-strain relations of these corroded specimens were not affected significantly when compared to the uncorroded specimens in the same series, as indicated in Fig. 10, particularly for the corroded Specimens AS1, AM1, AL1, BM1, BL1, CS1, and CM1. Furthermore, in the well-confined Specimens AS1, BS1, and CS1, those with small spacing of transverse reinforcement and high volumetric ratio of confining reinforcement, the corroded specimens still showed the ductile behavior after the maximum stress exceeded even though they were corroded. These specimens failed when the longitudinal reinforcing bars were buckled and the core concrete was crushed. Fig. 12 shows typical failure of some low corroded specimens with the corrosion level less than 10% after testing and taking out all the instruments. On the other hand, with the highly corroded specimens, where the corrosion level is greater than 15%, the severe pitting corrosion, or eventually the corrosion induced the fracture of transverse reinforcing bars can be observed. Fig. 13 demonstrates an example of some typical corroded transverse reinforcing bars of Specimen AS3 with the corrosion level of 25.0% after testing. In addition, it is of interest to notice that the severe pitting corrosion and corrosion induced fracture of transverse reinforcing bars occurred near the cover concrete crack regions. This is because the cracks of the cover concrete due to corrosion facilitated the chemical reaction between the ferrous ions and hydroxyl ions to form the corrosion products. It is also observed that the cracks induced by corrosion developed vertically along the direction of longitudinal reinforcement and occurred in the highly corroded specimens. Afterward, these cracks further developed and widened with the increase of the applied compression axial force during the test. Finally, these specimens failed with the fracture of transverse reinforcing bars and then the following buckling of the longitudinal reinforcement. Fig. 14 indicates the typical failure of some highly corroded specimens with the corrosion level greater than 20%. As demonstrated in Fig. 10, the severe pitting corrosion and the fracture of transverse reinforcing bars induced by corrosion significantly affected the stress-strain relations of highly corroded specimens. Particularly, more brittle behavior and steeper descending branches can be noticed in the complete stress-strain curves of these specimens.

4. Discussion of test results

4.1. Effect of corrosion level

The effect of corrosion level on the stress-strain relation of test specimens is demonstrated in Fig. 10. As observed, the initial stiffness was not significantly affected by the increase of corrosion level. However, the higher corrosion level resulted in the lower maximum concrete strength and the axial concrete strain at maximum strength. Furthermore, significant deterioration of confined strength after the maximum stress reached was more obvious with the increase of corrosion level for all cross sectional shapes, especially with the highly corroded specimens. For instance, comparing to the un-corroded Specimen AS0, an approximately 7.1%, 10.0%, 13.4% maximum confined strength reduction and 7.8%, 17.3%, 22.7% axial strain at maximum stress decrease for corroded Specimens AS1, AS2, and AS3 with the same cross sectional shape and reinforcement details were observed corresponding to the increase of their corrosion levels from 0% to 9.5%, 16.7%, and 25.0%, respectively. Although similar trends were also noticed for the other corroded specimens belong to Series B and C, their deterioration rates of strength and ductility are different, depending on the arrangements and spacing of confining reinforcement, as well as the cross sectional shapes of confined concrete. As predicted, the deterioration rate of strength and ductility after peak stress of corroded confined concrete constructed with large hoop spacing, low volumetric ratio, and highly corroded transverse reinforcement is much faster than that of corroded confined concrete with small hoop spacing, high volumetric ratio, and low corrosion level. The corrosion effect was more detrimental on the axial strain at maximum stress and ultimate axial strain than that on confined concrete strength.

4.2. Effect of volumetric ratio of transverse reinforcement

The volumetric ratio of transverse reinforcement is considered as one of the most significant parameters to improve the strength and ductility capacities of confined concrete. In this study, this effect on the stress-strain relations of corroded confined concrete under various corrosion levels can be observed in Fig. 10. For tested Specimens AS2, AM2, and AL3 with the corrosion levels of 16.7%, 12.5% and 17.5%, respectively, comparing to the un-corroded Specimens with the same design AS0, AM0, and AL0, an approximately 10.0%, 7.8%, 22.3% peak stress decrease and 13.8%, 20.0%, 31.3% ultimate axial strain reduction were observed corresponding to the volumetric ratio of transverse reinforcement of these specimens reduces from 2.51% to 1.57% and 0.97%, respectively. The experimental observation of the descending branches of stress-strain curves also revealed that among the corroded specimens subjected to the relatively similar corrosion levels, the lower volumetric transverse reinforcement ratio and larger hoop spacing resulted in more brittle behavior for corroded confined concrete. The similar trend can be also observed in Fig. 10 with corroded specimens belong to Series B and C. In conclusion, the volumetric ratio of transverse reinforcement significantly affects the stress-strain relations of corroded confined concrete, including the maximum strength, ultimate axial strain, as well as the descending

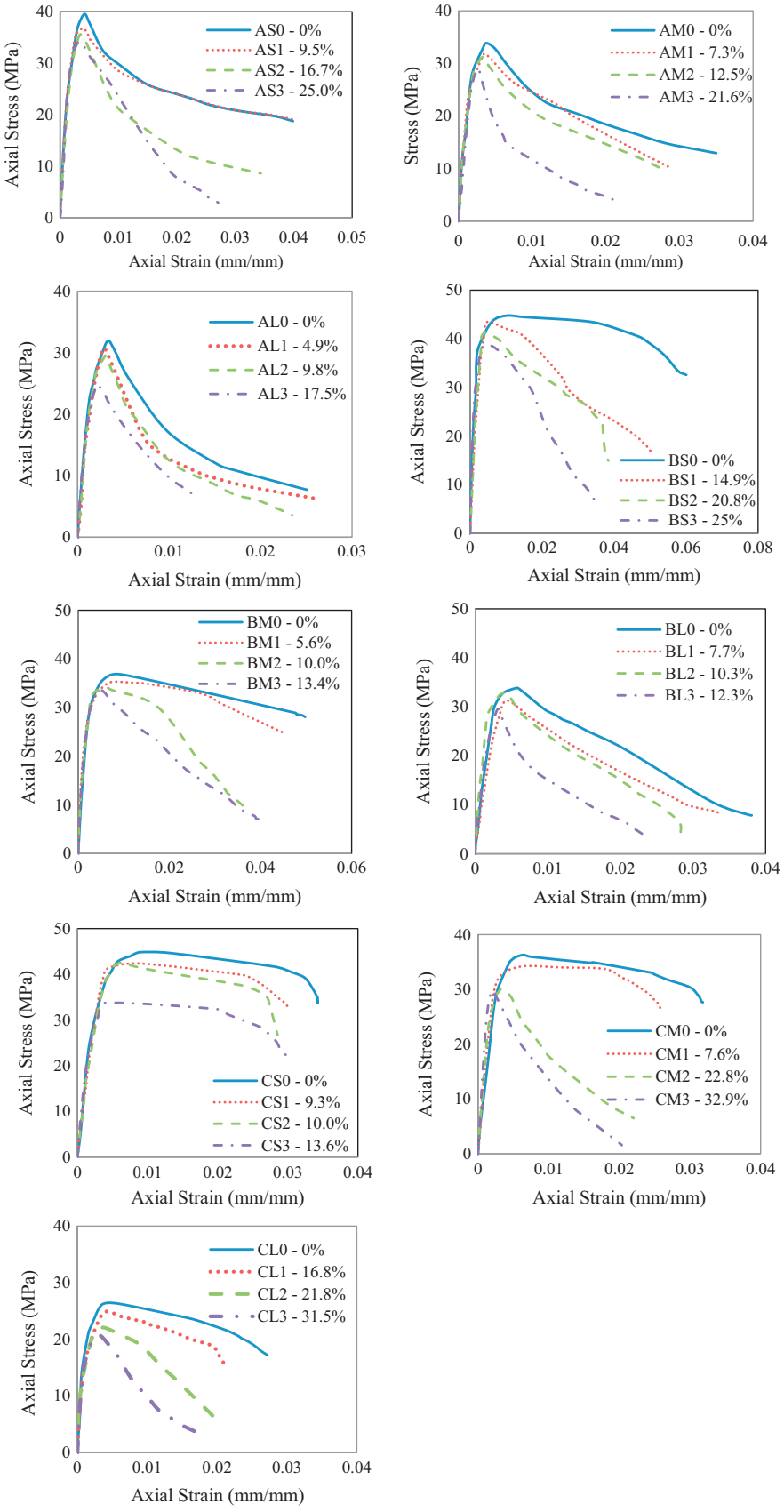

Fig. 10. Experimental stress-strain curves for confined concrete of test specimens subjected to various corrosion levels.

Fig. 11. Appearance of some typical corroded transverse reinforcing bars of specimen AS1 ($X_{corr} = 9.5\%$) after testing and removing all the rust.

AS1 ($X_{corr} = 9.5\%$) BM1 ($X_{corr} = 5.6\%$) CM1 ($X_{corr} = 7.6\%$)

Fig. 12. Appearance of specimens subjected to low corrosion levels after testing.

branches of stress-strain curves after exceeding the maximum strength.

4.3. Effect of confinement reinforcement configuration

It is well known that the transverse reinforcement arrangement is one of the vital factors that affect the performance of confined concrete because of its influence on the distribution of lateral confining pressure. However, this effect has not been well studied in cases of confined concrete undergo severe corrosive environment. In this study, the effect of transverse reinforcement arrangement can be observed by comparing the stress-strain relations of two pairs of corroded Specimens AM1&BL1, AS2&BM3, of almost the same volumetric ratio of transverse reinforcement and subjected to the similar corrosion levels. Specimens AM1 and AS2 were constructed using single perimeter hoops while Specimens BL1 and BM3 designed with double hoops configuration. Additionally, due to the compressive concrete strength varied among test specimens, the confined strength enhancement which is ratio of confined concrete strength to unconfined concrete strength is used to compare the confinement effectiveness of test specimens. The experimental results showed that both Specimens BL1 and BM3 performed better than AM1 and AS2 in terms of strength and ductility, as well as the improvement of deterioration rate after exceeding the maximum stress, for details, the enhancement of peak stress and ultimate strain of Specimen BL1 were 3.3% and 14.2% higher than those of Specimen AM1 while 7.6% and 14.5% higher of peak stress enhancement and ultimate strain can be also observed in Specimen BM3 compared to Specimen AS2. Therefore, these comparisons confirmed the improvement of strength and ductility in corroded concrete confined with double hoops configuration.

4.4. Effect of cross sectional shape of confined concrete

Generally, the normal concrete confined by circular spirals performs better than rectilinear ties because of its uniformly distributed confining pressure around the perimeter of the section. In this study, this effect was investigated and quantified for corroded circular and square specimens in terms of their strength and ductility. Comparing two pairs of the corroded Specimens CS1&AS1, CM1&AM1 which were designed with similar volumetric ratio of transverse reinforcement and under almost the same corrosion levels showed that the peak stress enhancements of circular corroded Specimens CS1 and CM2 were 15.0% and 10.6% higher than those of square corroded Specimens AS1 and AM1, respectively. In addition, these circular corroded specimens performed a ductile behavior after their peak stress attained while those square corroded specimens exhibited a pronounced reduction in load carrying capacity after the maximum load reached, showing that the cross sectional shape significantly affects the confinement effectiveness of corroded confined concrete.

5. Stress-strain model for confined concrete with corroded transverse reinforcement

5.1. Stress-strain relation

In this study, to establish the new analytical model for corroded confined concrete, the stress-strain model for un-corroded confined concrete proposed by Mander et al. [21] was adopted and modified to take into consideration the effects of corrosion because of some of its advantages, including the overall stress-strain curve can be represented by one single polynomial function and its application for any cross sectional shape of confined concrete. More importantly, comparing the well-known stress-strain models in literature [21,28–30] with the experimental results of un-corroded

Fig. 13. Appearance of some typical corroded transverse reinforcing bars of specimen AS3 ($X_{corr} = 25.0\%$) after testing and removing all the rust.

AS3 (X_{corr} = 25.0%) BS3 (X_{corr} = 25.0%) CM3 (X_{corr} = 32.9%)

Fig. 14. Appearance of specimens subjected to high corrosion levels after testing.

Specimens AL0, AM0, AS0, BL0, BM0, BS0, CL0, CM0, and CS0 in this study showed that the model proposed by Mander et al. [21] has the best interpretation of these experimental data, as indicated in Fig. 15. In the model for un-corroded confined concrete proposed by Mander et al. [21], the longitudinal compressive concrete stress f_c is expressed as follows:

$$f_c = \frac{f'_{cc} x r}{r - 1 + x^r} \tag{7}$$

$$x = \frac{\varepsilon_c}{\varepsilon_{cc}} \tag{8}$$

$$r = \frac{E_c}{E_c - E_{sec}} \tag{9}$$

$$E_c = 5000\sqrt{f'_{co}} \tag{10}$$

$$E_{sec} = \frac{f'_{cc}}{\varepsilon_{cc}} \tag{11}$$

where ε_c is the longitudinal compressive concrete strain; f'_{cc} and ε_{cc} are the maximum confined strength and corresponding axial strain, respectively, which will be modified later to take into consideration the effects of corroded transverse reinforcement; E_c and E_{sec} are the elasticity modulus of concrete and secant modulus of confined concrete at the maximum stress, respectively; f'_{co} is the maximum strength of unconfined concrete, which is estimated based on the experimental results, as shown in Table 1. When the experimental data is unavailable, the unconfined concrete strength f'_{co} can be expected to be equal 85% strength of the standard cylinder test results.

5.2. Maximum strength of corroded confined concrete

Generally, corrosion of reinforcement reduces the mechanical properties and diameter of reinforcement, resulting in the reduction of total cross-sectional area A_v and yield strength of transverse reinforcement f_{yh}. Therefore, a modification of volumetric ratio ρ_{sc} (Eq. (12)) and yield strength f^c_{yh} (Eq. (13)) for transverse reinforcement was made in this proposed model, resulting in the reduction of effective lateral confining pressure f'_l (Eq. (14)). Finally, based on the test data of 36 specimens, a regression analysis was conducted to modify the maximum confined strength f'_{cc} (Eq. (15)).

$$\rho_{sc} = (1 - X_{corr})\rho_s \tag{12}$$

$$f^c_{yh} = (1 - \alpha_s X_{corr}) f_{yh} \tag{13}$$

$$f'_l = \frac{1}{2} k_e \rho_{sc} f^c_{yh} \tag{14}$$

$$f'_{cc} = (1 - \alpha X_{corr}) f'_{co} \left(-1.254 + 2.254\sqrt{1 + \frac{7.94 f'_l}{f'_{co}}} - 2\frac{f'_l}{f'_{co}} \right) \tag{15}$$

where X_{corr} is the corrosion level in terms of mass loss of transverse reinforcement; α_s is the yield strength reduction factor for corroded transverse reinforcement, taken as 0.005 [14], $\alpha_s = 0.005$ was also recommended to use in [31]; α is stress correction coefficient derived from the regression analysis of the test data; $\alpha = 0.19$ for square confined section with single hoops configuration (Series A); $\alpha = 0.40$ for square confined section with double hoops configuration (Series B); $\alpha = 0.51$ for circular confined section with spiral hoops (Series C); k_e is the confinement effectiveness coefficient, more calculation details of this coefficient can be found in [21]. The average ratio of the measured maximum corroded confined strength of 36 specimens to their values calculated by using Eq. (15) is 0.997 and its standard deviation (SD) of 0.052, showing a good agreement between the experimental results and the proposed equation, as shown in Table 3 and Fig. 16.

5.3. Axial corroded concrete strain at maximum strength

As mentioned previously, the axial strain of corroded confined concrete corresponding to its maximum strength reduces significantly due to reinforcement corrosion, much more than the deterioration of maximum confined strength. Based on the experimental data of 36 specimens and regression analysis, the axial corroded concrete strain at the maximum stress ε_{cc} can be estimated for both circular and square confined sections with corroded transverse reinforcement, as follows:

$$\varepsilon_{cc} = (1 - \beta X_{corr})\varepsilon_{co} \left[1 + 5\left(\frac{f'_{cc}}{f'_{co}} - 1 \right) \right] \tag{16}$$

Basically, Eq. (16) was derived from modifying the original equation in [21] that takes into consideration the corrosion effect on the reduction of axial strain at peak stress. In this equation, β is strain correction coefficient; $\beta = 0.49$ for square confined section with single hoops configuration (Series A); $\beta = 1.29$ for square confined section with double hoops configuration (Series B); $\beta = 0.28$ for circular confined section with spiral hoops (Series C); ε_{co} is the axial strain of unconfined concrete corresponding to maximum unconfined stress, which is estimated based on the experimental results of unconfined concrete specimens, as indicated in Table 1. The value of $\varepsilon_{co} = 0.002$ can be assumed when the test data is not available. In this proposed equation, the strength of corroded confined concrete f'_{cc} is calculated following Eq. (15). The comparisons of axial corroded concrete strain between the experimental data and the proposed equation Eq. (16) produce a good agreement because the average ratio of measured axial corroded concrete strain at peak stress of 36 specimens to their values estimated by using Eq. (16) is 1.034 and its standard deviation (SD) of 0.176, as indicated in Table 3 and Fig. 17.

5.4. Ultimate strain of corroded confined concrete

It is conservative to estimate the ultimate strain of confined concrete corresponding to the strain at which the fracture of the first confining reinforcement occurs [21,32], causing longitudinal reinforcement to buckle and the crush of core concrete follows.

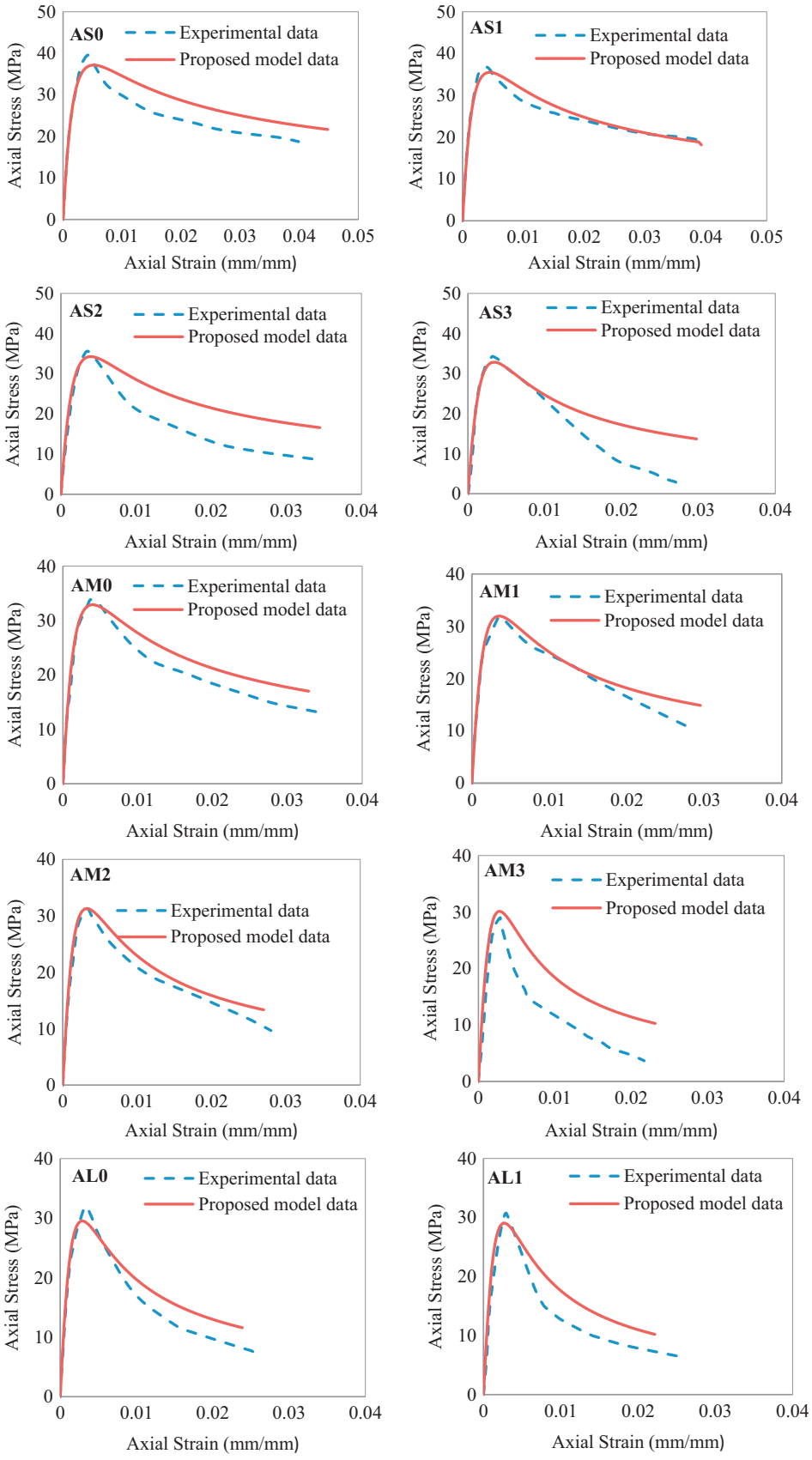

Fig. 15. Comparisons of experimental and analytical stress-strain curves for test specimens.

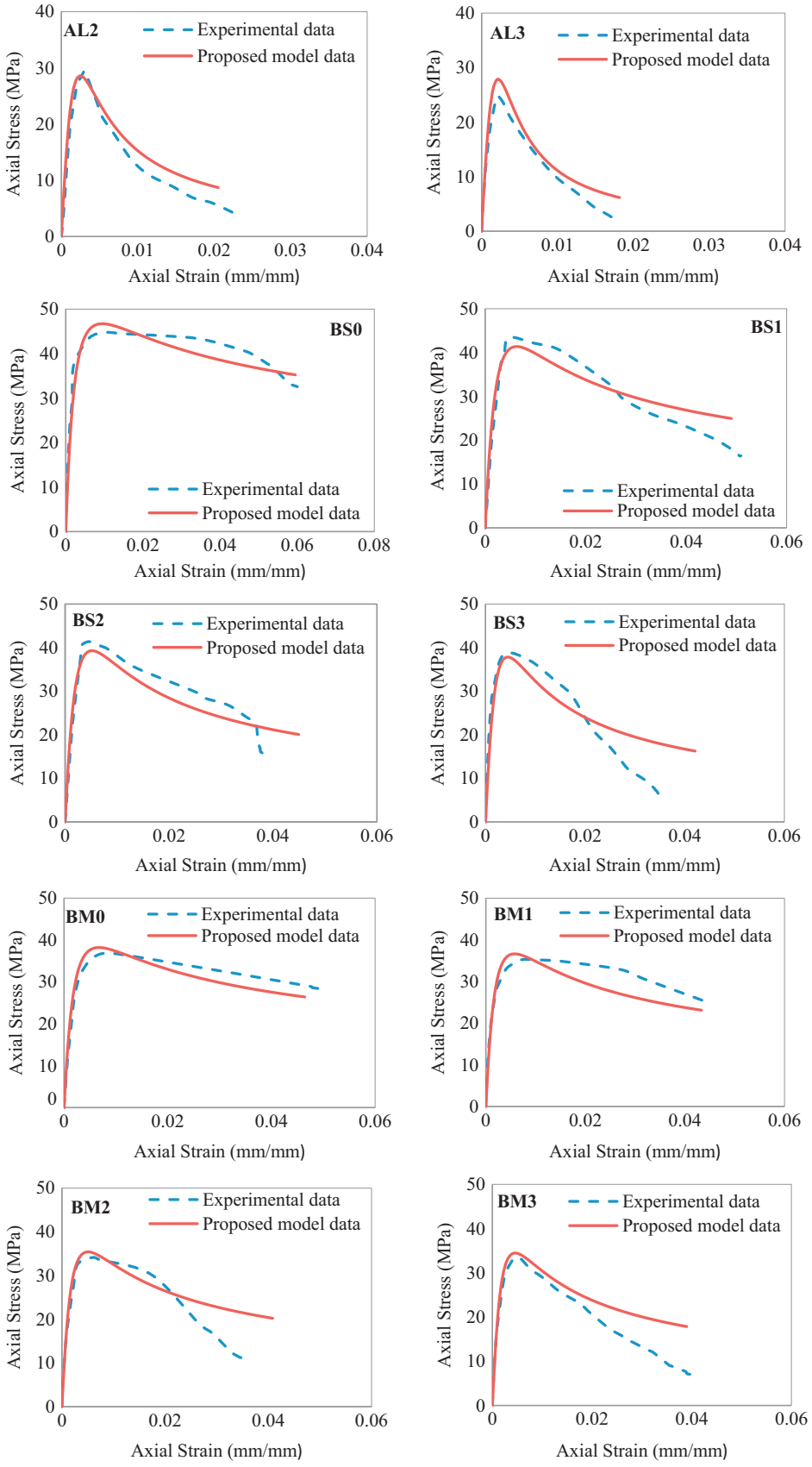

Fig. 15 (*continued*)

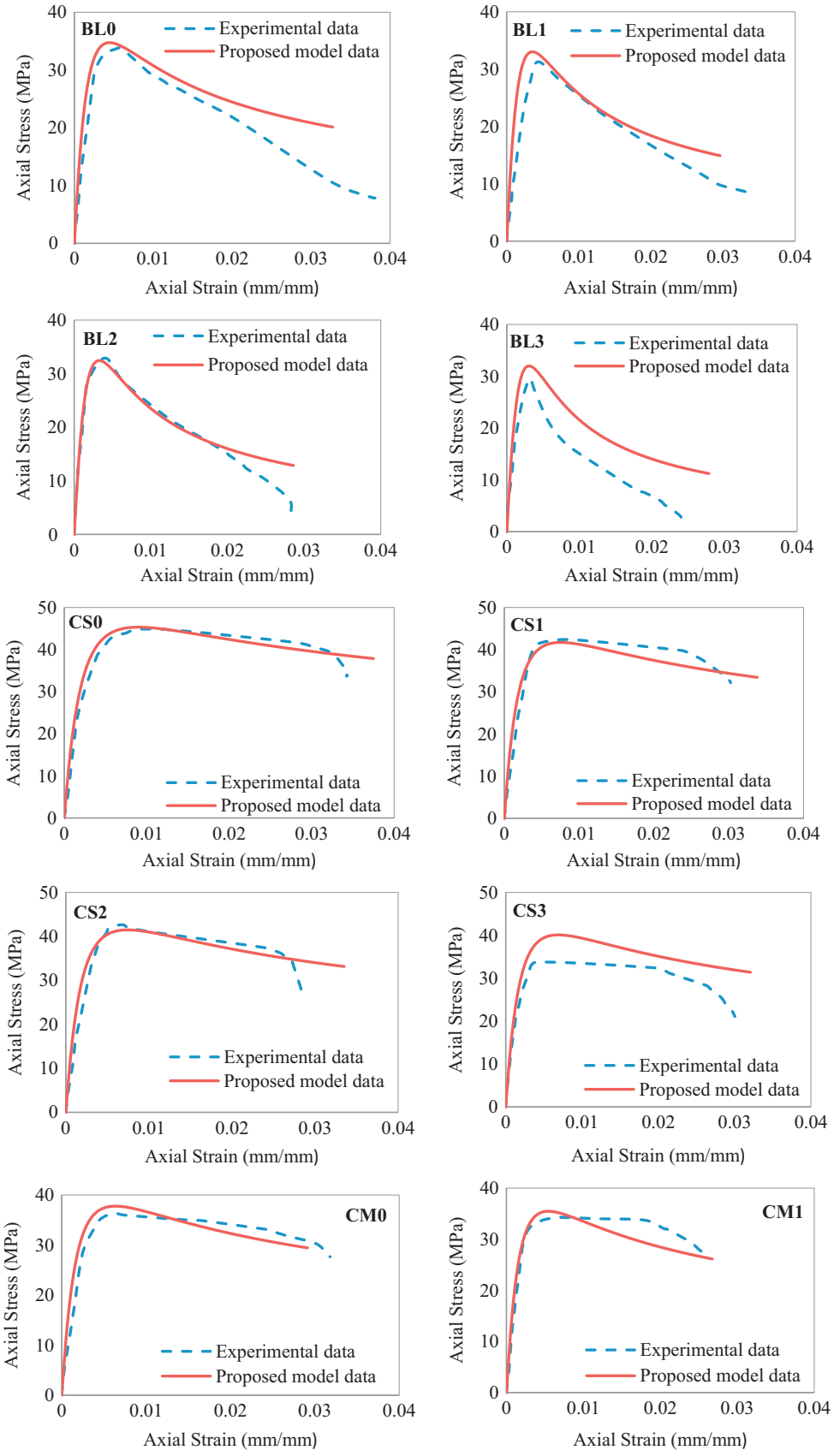

Fig. 15 (*continued*)

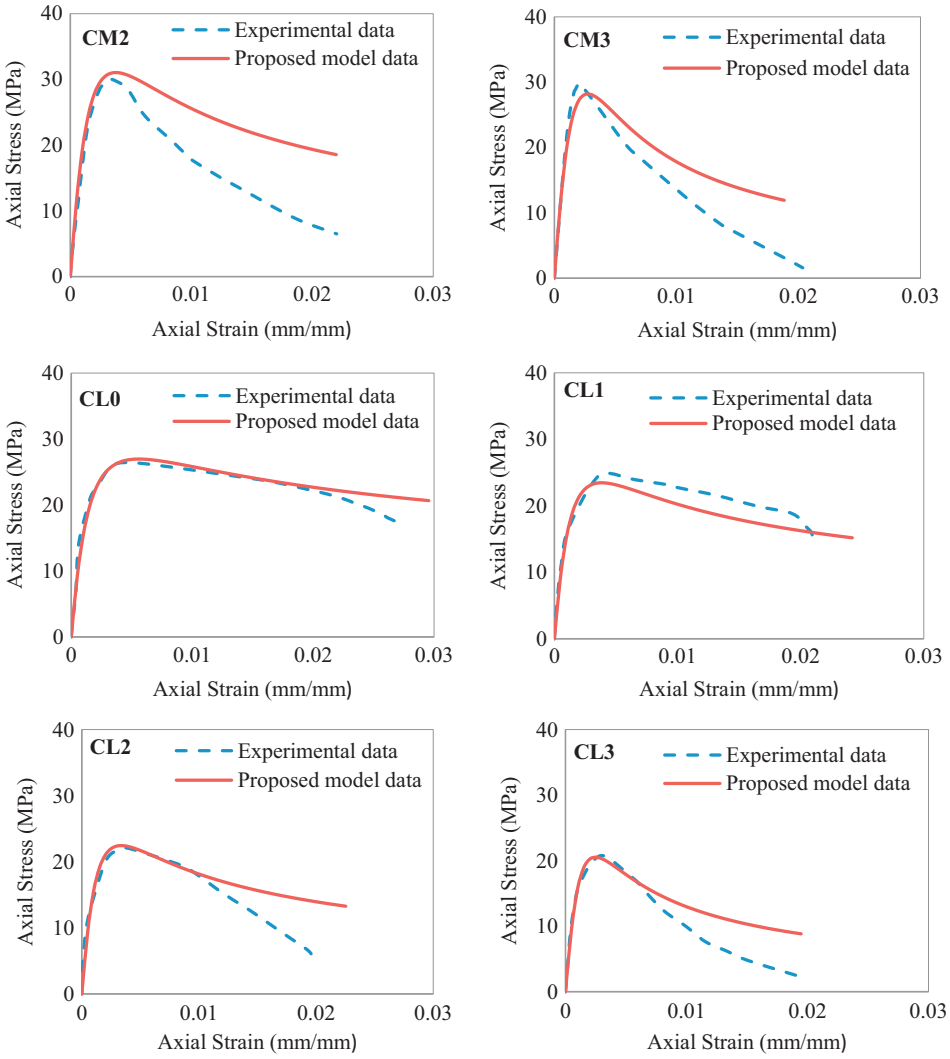

Fig. 15 (*continued*)

In order to predict the ultimate strain of corroded confined concrete ε_{cu}, the empirical equation proposed by Paulay and Priestley [32], which based on the energy balance approach, was adopted and modified as following:

$$\varepsilon_{cu} = 0.004 + (1 - X_{corr})\frac{1.4\rho_{sc} f^{c}_{yh} \varepsilon^{c}_{sm}}{f'_{cc}} \tag{17}$$

$$\varepsilon^{c}_{sm} = (1 - \beta_s X_{corr})\varepsilon_{sm} \tag{18}$$

where the modified volumetric ratio of transverse reinforcement ρ_{sc} and the strength of corroded confined concrete f'_{cc} are estimated following Eqs. (12) and (16); f^{c}_{yh} is the yield strength of corroded transverse calculated based on Eq. (13); ε^{c}_{sm} and ε_{sm} are the steel strains at the maximum tensile stress of corroded and un-corroded transverse reinforcement, respectively; $\varepsilon_{sm} = 0.12$ is adopted in this study based on the test result. β_s is the ultimate strain reduction factor for corroded transverse reinforcement, taken as 0.05 [15]. Table 3 and Fig. 18 show a good correlation between the measured ultimate strain of corroded concrete of 36 specimens and their predicted values using Eq. (17), particularly the average ratio of the test data to the predicted results is 0.985 and its standard deviation (SD) of 0.095.

Fig. 15 demonstrates the comparisons of complete stress-strain curves of 36 specimens between the experimental data and the proposed analytical model that illustrated a reasonably good prediction of this proposed model. Furthermore, the normalized corroded concrete stress error E_{stress} was evaluated to quantify the accuracy of the proposed analytical model that is the error between measured and calculated corroded concrete stress error, as the following equation:

$$E_{stress} = \frac{1}{\max(|F^{i}_{mea}|)}\sqrt{\frac{1}{n}\sum_{i=1}^{n}\left(F^{i}_{mea} - F^{i}_{cal}\right)^2} \tag{19}$$

where F_{mea} and F_{cal} are the measured and calculated corroded concrete stresses at the i^{th} loading step. Table 3 summarizes the values of normalized corroded concrete stress error of 36 specimens. As indicated, the mean error in corroded concrete stress of 36 specimens is 11.28%, showing a reasonable estimation of the overall stress-strain curves for corroded confined concrete by adopting this proposed model.

6. Conclusions

In this paper, the influences of the corroded transverse reinforcement on the stress-strain relation of confined concrete are experimentally and analytically investigated. The key parameters affecting the stress-strain relation of confined concrete with corroded transverse reinforcement are investigated and quantified,

Table 3
Experimental results and comparisons with proposed analytical model.

Unit	f'^{exp}_{cc} (MPa)	f'^{pro}_{cc} (MPa)	$\frac{f'^{exp}_{cc}}{f'^{pro}_{cc}}$	ε^{exp}_{cc} (%)	ε^{pro}_{cc} (%)	$\frac{\varepsilon^{exp}_{cu}}{\varepsilon^{pro}_{cc}}$	ε^{exp}_{cu} (%)	ε^{pro}_{cu} (%)	$\frac{\varepsilon^{exp}_{cu}}{\varepsilon^{pro}_{cu}}$	E_{stress} (%)
AL0	31.96	29.51	1.083	0.331	0.289	1.145	2.607	2.381	1.095	7.07
AL1	30.62	29.05	1.054	0.300	0.268	1.119	2.582	2.217	1.165	11.84
AL2	29.49	28.59	1.032	0.305	0.248	1.229	2.347	2.056	1.142	8.46
AL3	24.83	27.86	0.891	0.218	0.217	1.005	1.792	1.815	0.987	11.27
AM0	33.85	32.91	1.029	0.373	0.396	0.941	3.501	3.287	1.065	6.41
AM1	31.84	31.95	0.996	0.351	0.353	0.993	2.867	2.942	0.974	4.84
AM2	31.20	31.29	0.997	0.344	0.324	1.060	2.800	2.710	1.033	5.36
AM3	29.01	30.12	0.963	0.286	0.276	1.035	2.168	2.315	0.937	17.56
AS0	39.57	37.17	1.065	0.421	0.520	0.810	3.988	4.489	0.888	7.58
AS1	36.78	35.51	1.036	0.388	0.448	0.867	4.019	3.887	1.034	3.35
AS2	35.61	34.27	1.039	0.348	0.397	0.877	3.437	3.631	0.947	12.54
AS3	34.27	32.83	1.044	0.325	0.341	0.953	2.706	2.970	0.911	17.46
BL0	33.84	34.74	0.974	0.582	0.446	1.304	3.809	3.273	1.164	14.20
BL1	32.28	33.03	0.977	0.433	0.356	1.218	3.343	2.966	1.127	18.39
BL2	32.91	32.45	1.014	0.407	0.327	1.244	2.824	2.862	0.987	12.06
BL3	29.55	31.99	0.924	0.313	0.306	1.022	2.401	2.781	0.864	19.98
BM0	36.89	38.20	0.966	0.851	0.672	1.266	4.979	4.645	1.072	5.91
BM1	35.26	36.64	0.962	0.728	0.577	1.262	4.512	4.335	1.041	7.05
BM2	34.15	35.40	0.965	0.612	0.506	1.209	3.608	4.088	0.883	18.72
BM3	33.59	34.46	0.975	0.490	0.456	1.074	4.021	3.902	1.031	16.78
BS0	44.77	46.72	0.958	1.034	0.947	1.092	6.005	5.954	1.009	6.57
BS1	43.45	41.37	1.050	0.472	0.625	0.755	5.090	4.901	1.039	9.11
BS2	41.38	39.29	1.053	0.456	0.517	0.882	3.837	4.492	0.854	7.89
BS3	38.45	37.83	1.016	0.365	0.447	0.815	3.531	4.205	0.840	18.99
CL0	26.33	26.97	0.976	0.574	0.559	1.028	2.721	2.962	0.919	7.85
CL1	24.90	23.47	1.061	0.409	0.384	1.065	2.099	2.422	0.867	5.43
CL2	22.04	22.45	0.982	0.396	0.336	1.180	1.957	2.260	0.866	19.50
CL3	20.67	20.53	1.007	0.328	0.248	1.321	1.915	1.952	0.981	18.04
CM0	36.30	37.76	0.961	0.647	0.635	1.019	3.183	2.916	1.091	7.50
CM1	34.21	35.47	0.964	0.627	0.544	1.152	2.630	2.678	0.982	7.46
CM2	30.06	31.04	0.968	0.335	0.376	0.893	2.202	2.203	0.999	19.17
CM3	29.87	28.19	1.060	0.201	0.274	0.734	2.035	1.889	1.078	14.37
CS0	44.84	45.32	0.989	0.899	0.899	1.000	3.424	3.754	0.912	6.47
CS1	42.39	41.72	1.016	0.877	0.753	1.165	3.026	3.379	0.895	7.62
CS2	42.65	41.48	1.028	0.689	0.744	0.926	2.854	3.355	0.851	7.56
CS3	33.75	40.11	0.841	0.401	0.690	0.581	3.004	3.209	0.936	15.85
Mean			0.997			1.034			0.985	11.28
Coefficient of variation			0.052			0.176			0.095	

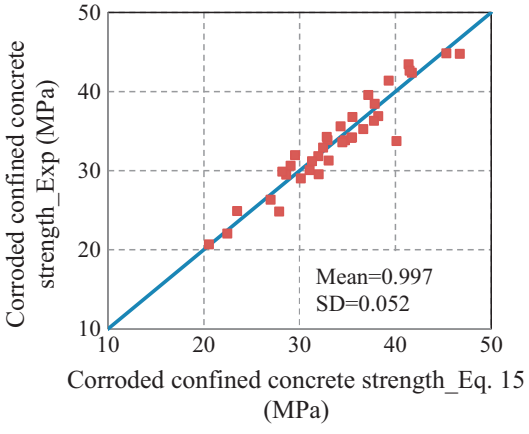

Fig. 16. Comparisons of the corroded confined concrete strength of 36 specimens between experimental results and calculated by Eq. (15).

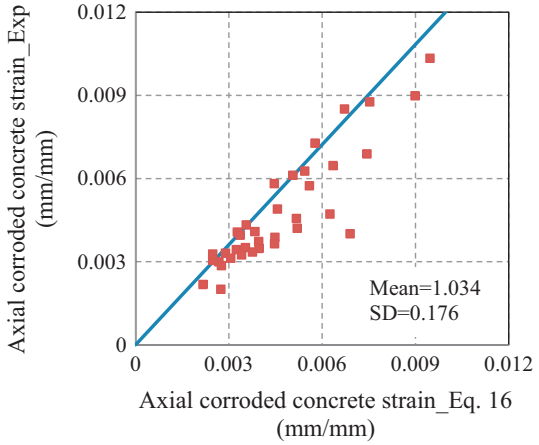

Fig. 17. Comparisons of the axial corroded concrete strain at maximum strength of 36 specimens between experimental results and calculated by Eq. (16).

including corrosion level, volumetric ratio, arrangement and configuration of confining reinforcing bars, and cross sectional shape of confined concrete. Some important conclusions can be summarized from the experimental and analytical studies as followings:

1. A stress-strain model for confined concrete with corroded transverse reinforcement is proposed by incorporating the corrosion effects into the model for un-corroded confined concrete proposed by Mander et al. [21]. The proposed model showed a reasonably good estimate of the experimental stress-strain curves for both circular and square specimens with various corrosion levels of transverse reinforcement and subjected to compression axial loading.
2. The experimental results revealed that the corrosion level and the volumetric ratio of transverse reinforcement are the most important factors affecting the stress-strain relations of corroded confined concrete. As the corrosion level increases, both

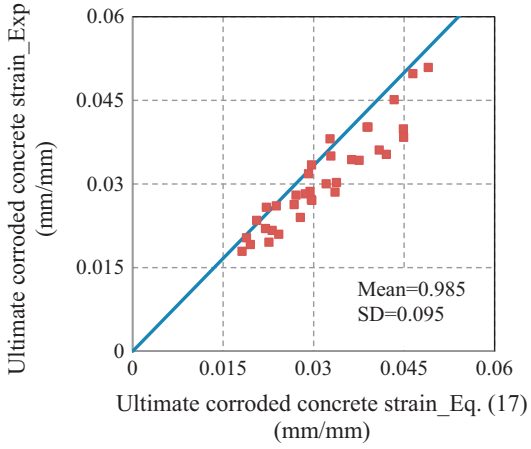

Fig. 18. Comparisons of ultimate corroded concrete strain of 36 specimens between experimental results and calculated by Eq. (17).

strength and ductility of the corroded confined concrete drastically decrease and the slope of the stress-strain curve after exceeding the maximum stress also becomes steeper. The corrosion effect on the corroded confined concrete is found to be more detrimental on the axial strain at the maximum stress and ultimate strain than that on the maximum strength.

3. The pitting corrosion is more significant with the increase of corrosion level which significantly affects the overall stress-strain relations of corroded confined concrete. Particularly, as observed in corroded specimens with corrosion levels in terms of mass loss less than approximately 10%, the uniform corrosion of transverse reinforcement slightly influenced their global stress-strain relations of corroded confined concrete. In addition, at the end of the test, neither the cover concrete crack induced by corrosion nor the fracture of transverse reinforcing bars was observed in these corroded specimens. However, with the highly corroded specimens under corrosion levels from 15% to 30%, the severe pitting corrosion can be noticed which resulted in the significant deterioration of the strength and ductility of corroded confined concrete. This is because of the severe reduction of the confinement effectiveness caused by the fracture of confining transverse reinforcement due to severe pitting corrosion.
4. Regarding the effect of cross sectional shape of confined concrete, the experimental results showed that with the similar volumetric ratio of transverse reinforcement and under the same corrosion levels, the corroded concrete confined with circular spirals performed better than that confined with rectilinear ties in terms of both strength and ductility capacity. In addition, more ductile behavior was also observed for the corroded concrete confined with circular spirals even though subjected to relatively high corrosion levels.
5. The experimental results also confirmed that the corroded concrete confined with double hoops configuration, resulting in the uniform distribution of confinement pressure, significantly improved the confinement effectiveness, particularly the increase of the maximum strength and ultimate concrete strain, as well as delay in the deterioration rate of the stress-strain curves after exceeding the maximum stress, comparing to the corroded concrete confined with single hoops configuration.

Acknowledgements

The financial support received from the National Natural Science Foundation of China (51368006 and 51668008) is gratefully acknowledged.

References

[1] Jaffer SJ, Hansson CM. Chloride-induced corrosion products of steel in cracked-concrete subjected to different loading conditions. Cem Concr Res 2009;39:116–25.
[2] Çağatay İH. Experimental evaluation of buildings damaged in recent earthquakes in Turkey. Eng Fail Anal 2005;12:440–52.
[3] Alipour A, Shafei B, Shinozuka M. Performance evaluation of deteriorating highway bridges located in high seismic areas. J Bridge Eng 2011;16:597–611.
[4] Mangat PS, Elgarf MS. Flexural strength of concrete beams with corroding reinforcement. ACI Struct J 1999;96:149–58.
[5] Torres-Acosta AA, Navarro-Gutierrez S, Terán-Guillén J. Residual flexure capacity of corroded reinforced concrete beams. Eng Struct 2007;29:1145–52.
[6] Ou Y-C, Chen H-H. Cyclic behavior of reinforced concrete beams with corroded transverse steel reinforcement. J Struct Eng 2014;140:04014050.
[7] El-Sayed AK, Shuraim AB, Hussain RR. Influence of stirrup corrosion on shear strength of reinforced concrete slender beams. ACI Struct J 2016;113:1223–32.
[8] Meda A, Mostosi S, Rinaldi Z, Riva P. Experimental evaluation of the corrosion influence on the cyclic behaviour of RC columns. Eng Struct 2014;76:112–23.
[9] Yang SY, Song XB, Jia HX, Chen X, Liu XL. Experimental research on hysteretic behaviors of corroded reinforced concrete columns with different maximum amounts of corrosion of rebar. Constr Build Mater 2016;121:319–27.
[10] Goksu C, Ilki A. Seismic behavior of reinforced concrete columns with corroded deformed reinforcing bars. ACI Struct J 2016;113:1053–64.
[11] Bousias SN, Triantafillou TC, Fardis MN, Spathis L, O'Regan BA. Fiber-reinforced polymer retrofitting of rectangular reinforced concrete columns with or without corrosion. ACI Struct J 2004;101:512–20.
[12] Li J, Gong J, Wang L. Seismic behavior of corrosion-damaged reinforced concrete columns strengthened using combined carbon fiber-reinforced polymer and steel jacket. Constr Build Mater 2009;23:2653–63.
[13] Meda A, Mostosi S, Rinaldi Z, Riva P. Corroded RC columns repair and strengthening with high performance fiber reinforced concrete jacket. Mater Struct 2016;49:1967–78.
[14] Du YG, Clark LA, Chan AHC. Residual capacity of corroded reinforcing bars. Mag Concr Res 2005;57:135–47.
[15] Du YG, Clark LA, Chan AHC. Effect of corrosion on ductility of reinforcing bars. Mag Concr Res 2005;57:407–19.
[16] Stewart MG. Mechanical behaviour of pitting corrosion of flexural and shear reinforcement and its effect on structural reliability of corroding RC beams. Struct Saf 2009;31:19–30.
[17] Apostolopoulos CA, Demis S, Papadakis VG. Chloride-induced corrosion of steel reinforcement – mechanical performance and pit depth analysis. Constr Build Mater 2013;38:139–46.
[18] Kashani MM, Lowes LN, Crewe AJ, Alexander NA. Phenomenological hysteretic model for corroded reinforcing bars including inelastic buckling and low-cycle fatigue degradation. Comput Struct 2015;156:58–71.
[19] Ou Y-C, Susanto YTT, Roh H. Tensile behavior of naturally and artificially corroded steel bars. Constr Build Mater 2016;103:93–104.
[20] Kashani MM. Size effect on inelastic buckling behavior of accelerated pitted corroded bars in porous media. J Mater Civ Eng 2017;29:1–13.
[21] Mander JB, Priestley MJN, Park R. Theoretical stress-strain model for confined concrete. J Struct Eng New York, NY 1988;114:1804–26.
[22] Li B, Park R, Tanaka H. Stress-strain behavior of high-strength concrete confined by ultra-high- and normal-strength transverse reinforcements. ACI Struct J 2001;98:395–406.
[23] ASTM G1-03. Standard practice for preparing, cleaning, and evaluating corrosion test specimens. West Conshohocken, PA, USA; 2003.
[24] Mander JB, Priestley MJN, Park R. Observed stress-strain behavior of confined concrete. J Struct Eng New York, NY 1988;114:1827–49.
[25] Li B. Strength and ductility of reinforced concrete members and frames constructed using high strength concrete. Phd thesis. Christchurch (New Zealand): Dept. of Civil Engineering, Univ. of Canterbury; 1994.
[26] Dodd LL, Cooke N. The dynamic behavior of reinforced-concrete bridge piers subjected to New Zealand seismicity. Research report. New Zealand: Department of Civil Engineering, University of Canterbury; 1992. p. 460.
[27] Hsu TTC, Mo YL. Unified theory of concrete structures. Chichester (West Sussex, UK) and Hoboken (NJ): Wiley; 2010.
[28] Scott BD, Park R, Priestley MJN. Stress-strain behavior of concrete confined by overlapping hoops at low and high strain rates. J Am Concr Inst 1982;79:13–27.
[29] Saatcioglu M, Razvi S. Strength and ductility of confined concrete. J Struct Eng 1992;118:1590–15607.
[30] Hoshikuma J, Kawashima K, Nagaya K, Taylor A. Stress-strain model for confined reinforced concrete in bridge piers. J Struct Eng 1997;123:624–33.
[31] Stewart MG, Al-Harthy A. Pitting corrosion and structural reliability of corroding RC structures: experimental data and probabilistic analysis. Reliability Eng Syst Saf 2008;93:373–82.
[32] Paulay T, Priestley MJN. Seismic design of reinforced concrete and masonry buildings. New York: Wiley; 1992.